

Dynamic Covalent Properties of a Novel Indolo[3,2-b]carbazole Diradical

Irene Badía Domínguez,^[a] Miriam Peña Álvarez,^{[b]1} Deliang Wang,^[c] Andrés Pérez Guardiola,^[d] Yolanda Vida,^[e,f] Sandra Rodríguez González,^[a] Juan T. López Navarrete,^[a] Víctor Hernández Jolín,^[a] Juan C. Sancho García,^[d] Valentín García Baonza,^[g] Rosie Nash,^[h] František Hartl,^{[h]*} Hongxiang Li,^{[c]*} M. Carmen Ruiz Delgado ^{[a]*}

[a] Department of Physical Chemistry, University of Málaga, Campus de Teatinos s/n, 229071, Málaga, Spain.

[b] Centre for Science at Extreme Conditions & School of Physics and Astronomy, University of Edinburgh, Edinburgh EH9 3FD, United Kingdom.

[c] Key Laboratory of Synthetic and Self-assembly Chemistry for Organic Functional Materials, Shanghai Institute of Organic Chemistry, Chinese Academy of Sciences, Shanghai, 200032, China.

[d] Department of Physical Chemistry, University of Alicante, E-03080 Alicante, Spain.

[e] Universidad de Málaga - IBIMA, Dpto. Química Orgánica, Campus de Teatinos s/n, 29071 Málaga, Spain.

[f] Centro Andaluz de Nanomedicina y Biotecnología-BIONAND. Parque Tecnológico de Andalucía, C/ Severo Ochoa, 35, 29590 Campanillas, Málaga, Spain

[g] MALTA-Consolider Team and Instituto de Geociencias IGEO (CSIC-ICM), University Complutense of Madrid, 28040 Madrid, Spain

[h] Department of Chemistry, University of Reading, Whiteknights, Reading RG6 6DX, United Kingdom. E-mail: f.hartl@reading.ac.uk

Abstract

This work describes the synthesis and properties of a dicyanomethyl-substituted indolo[3,2-b]carbazole diradical **ICz-CN**. This quinoidal system dimerises almost completely to **(ICz-CN)₂** containing two long C(sp³)-C(sp³) σ -bonds between the dicyanomethyl units, formed by coupling between the unpaired electrons in diradical **ICz-CN**. **(ICz-CN)₂** exhibits a pancake structure with the two indolocarbazole (**ICz**) backbones in an antiparallel sandwich conformation, as revealed by IR and Raman spectroscopies and DFT calculations. The cyclic voltammetric and UV-vis spectroelectrochemical data, and comparison with reference monomer **ICz-Br** reveal that the nature of the reversible oxidation of **(ICz-CN)₂** at ambient temperature and **ICz-CN** at elevated temperature is very similar in all these compounds due to the prevailing localization of their HOMO on the **ICz** backbone. The involvement of the dicyanomethylene groups stabilizes the close-lying LUMO and LUMO+1 of **(ICz-CN)₂** and especially **ICz-CN** compared to **ICz-Br**, resulting in the distinctive cathodic behaviour at low overpotentials. Differently from neutral **ICz-CN**, its radical anion and dianion are remarkably stable at ambient conditions. The UV-Vis(-NIR) electronic transitions in parent **(ICz-CN)₂** and **ICz-CN** and their different redox forms have been assigned convincingly with the aid of TD-DFT calculations. The σ -bond cleavage in neutral **(ICz-CN)₂** is achieved in solution and in the solid-state upon soft external stimuli (time, temperature, pressure), showing a strong chromism from light yellow to blue-green. Interestingly, the solvent nature strongly determines the temperature range and rate of the reversible σ -dimerization. The dynamic covalent properties in the solid-state are best described by the formation of open linear staircase oligomers under mild non-hydrostatic

¹ Work conducted when Miriam Peña-Alvarez was a team member of MALTA-Consolider Team, Department of Physical Chemistry I, Chemistry Faculty, University Complutense of Madrid, 28040 Madrid, Spain

stresses (*i.e.*, grinding) while the monomeric diradical species are predominantly achieved under high hydrostatic pressure conditions (>1 GPa).

Introduction

Chromo-active materials have attracted much interest of the scientific community in different fields as they are able to reversibly change colour when (i) exposed to certain light energies (photochromic switches)¹, (ii) slightly deformed with small compressive strain² or (iii) lightly heated/cooled.³ The reversible homolytic covalent bond cleavage/formation involving radical species has been recently demonstrated to be an efficient strategy to obtain multi-responsive chromic soft materials.³⁻⁴ Owing to this property, organic mono- and diradicals have emerged as essential building blocks in Dynamic Covalent Chemistry (DCC).⁵ The unique feature of the open-shell systems to form weak self-assembled molecular complexes has earmarked organic radicals as prospective for a great number of applications such as stimuli-responsive soft materials,³ spintronics⁶, spin cross-over materials⁷ or molecular self-assembly.⁸

Currently, several dicyanomethyl-substituted compounds have been identified to undergo reversible σ -oligomerization through the formation of long $(\text{CN})_2\text{C}-\text{C}(\text{CN})_2$ σ -bonds, giving rise to cyclophanes and other macrocyclic compounds.^{2a, 3, 4d, 4h, 9} For instance, our teams have found that carbazole-based diradicals are able to form stable cyclophane macrocycles upon soft external stimuli, showing a strong chromic effect from violet to white.^{3b} In another recent study, we have explained how the different substitution positions of the dicyanomethylene groups affect the self-assembly of carbazole-based diradicals.^{3c} Meta-substituted cyclophanes were found to dissociate harder both in solution and in the solid state when compared to para-substituted carbazole homologues, as a result of the formation of more stable macrocycles with shorter C-C bonds in the bridge. However, a fundamental understanding of how an enlargement of the conjugated core affects the intermolecular σ -bonding reactivity of carbazole-based diradicals is still missing.

It is worth noticing that particularly indolocarbazole-based systems have been studied in depth because of their promising properties, *viz.*: (i) good planarity and rigid conjugated core, which can increase the charge transport properties by improving intermolecular interactions reflected in better molecular packing arrangements; (ii) high thermal stability; (iii) prominent photophysical and electrochemical properties, such as wide band gap and low-lying HOMOs, which outlines them as promising materials for organic electronics.¹⁰

Hitherto, five different indolocarbazole isomers have been distinguished by the position and orientation of the nitrogen atom corresponding to the indole moiety change (see Figure S1). Although other possible configurations also exist, these are rather rare and usually not incorporated in the “classical” indolocarbazole concept.¹¹ In particular, the chemistry of indolo[3,2-*b*]carbazole has frequently been reported in the literature,¹² evidencing a quinoidal character for its ground state¹³ and an easy modulation of their properties by the insertion of functional groups.¹⁴ However, the introduction of dicyanomethylene terminal groups, a well-known strategy to stabilize diradical species, has not been explored so far in these materials. All these properties make indolocarbazole-based systems ideal test-bed molecules for the design of new diradical compounds.

In the present work, we have synthesized and characterized an indolo[3,2-*b*]carbazole compound containing terminal dicyanomethylene groups in the 3,9-positions, abbreviated as **ICz-CN**, which is capable of forming a σ -dimer structure with two co-facial

indolocarbazole units featuring attractive π - π interactions (Figure 1). Our study will focus on the relation between the diradical character of the open-shell monomers and the σ -oligomerization also referred as cyclophane formation (**ICz-CN** to **(ICz-CN)₂**). In addition, the reversibility of the monomer/cyclophane transformation will also be explored both in: (i) solid state by varying the external stimuli (temperature and pressure), and (ii) in solution where solvents of different polarity and cyclovoltammetry will be employed to infer molecular connectivity. A combined experimental and theoretical approach to reach the goals will couple a range of spectroscopic techniques and cyclic voltammetry with density functional theory (DFT) calculations.

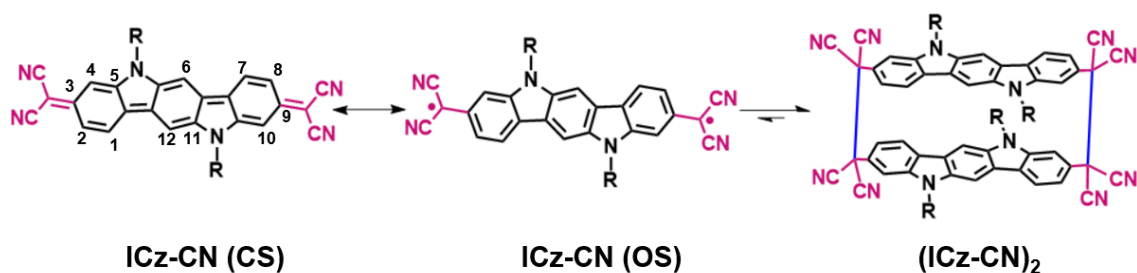
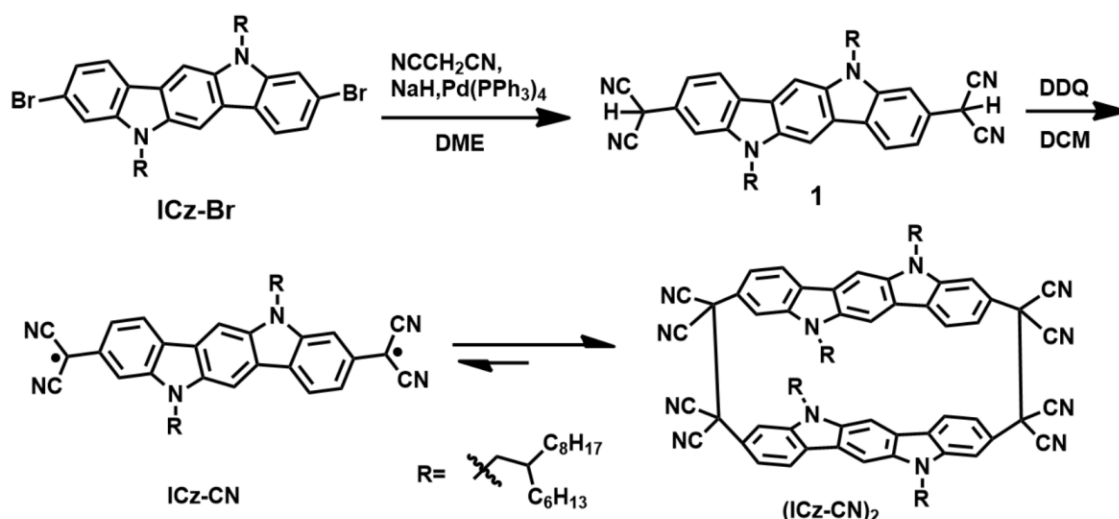


Figure 1. Equilibrium between the isolated monomer **ICz-CN** and its corresponding σ -dimer **(ICz-CN)₂**. The singlet ground state of **ICz-CN** is presented as a resonance between the closed-shell (CS) state (left) and the open-shell (OS) diradical state (middle).

Results and Discussion

1. Syntheses

The synthetic route to **ICz-CN** and the σ -stacked dimer **(ICz-CN)₂** is shown in Scheme 1 (see Supporting Information for the complete experimental details). In the initial step, 3,9-dibromo-indolo[3,2-b]carbazole (**ICz-Br**) reacted with malononitrile through a typical Pd-catalysed Takahashi coupling reaction to afford precursor **1**. After oxidation of **1** with 2,3-dichloro-5,6-dicyanobenzoquinone (DDQ), **ICz-CN** was obtained and concomitantly dimerized in part to **(ICz-CN)₂** in solution due to its active diradical character. Similar to our previously reported 2,7-dicyanomethylene-9-(2-ethylhexyl)carbazole diradical, **Cz-CN^{3b}** (see Figure S2), an equilibrium exists between **ICz-CN** and **(ICz-CN)₂** in solution, with the dominant the dimer contribution evidenced by electronic absorption spectroscopy at variable temperature, UV-Vis-NIR spectroelectrochemistry and HPLC results (see Figure S4) in connection with DFT and TD DFT calculations (see the discussion in the relevant sections below).



Scheme 1. The synthetic route to diradical **ICz-CN** in equilibrium with the corresponding cyclophane **(ICz-CN)₂**.

2. Cyclophane Structural Features

The reactive diradicals can form linear polymer or cyclophane structures. The long retention time of GPC (see Figure S4) excludes linear polymerization of **ICz-CN** diradical. **ICz-CN** compounds and its precursor **ICz-Br** were examined by diffusion NMR techniques. Diffusion-ordered spectroscopy (DOSY) experiments were carried out at **ICz** compounds concentration below 2 mM, which corresponds to a dilute regime where the intermolecular separation avoids aggregate formation. Diffusion coefficients (D) were determined and used to estimate the size of the molecules in solution, by calculating the hydrodynamic radius (R_h) using the Stokes-Einstein equation: $R_h = k_B T / 6\pi\eta D$, where k_B is the Boltzmann constant, T is the temperature and η is the kinematic viscosity of the solution.¹⁵

Larger structures diffuse more slowly in solution, showing smaller diffusion coefficients. As can be observed in Table 1, **ICz-CN** present a smaller diffusion coefficient than **ICz-Br** and for instance a higher R_h . This indicates that the estimated size of the CN derivative is slightly more than twice larger than that of the Br derivative, in line with the formation of a dimeric structure in the case of **ICz-CN**. This is in good analogy with the well-known trend in diradical systems to form weak and long C-C single bonds in the process of co-facial coupling between the radical centres, giving rise to the formation of σ -aggregates.^{3c, 9a, 16}

Table 1. Diffusion coefficients (D) and hydrodynamic radii (R_h) determined by diffuse NMR experiments.

Compound	D (m^2s^{-1})	R_h (\AA)
ICz-Br	$4.05 \cdot 10^{-10}$	10
(ICz-CN)₂	$1.76 \cdot 10^{-10}$	23

With the aim of predicting the most favourable intermolecular arrangement of the σ -dimer aggregate, we performed DFT calculations for different dimer conformations¹⁷ (Figure 2a): (i) an antiparallel arrangement of the two **ICz-CN** chains; and (ii) a parallel orientation with co-facially superimposed units, thereby maximizing the orbital overlap between the

π -conjugated cores.¹⁸ The calculated free energies revealed that **ICz-CN** is able to form a pancake dimer structure resulting from attractive π - π interactions between two indolocarbazole backbones (see Figure 2a and Figure S5). When comparing the two dimer models, the formation of the antiparallel configuration (Figure 2a, top) is found to be 17 kcal mol⁻¹ more favourable than the parallel one. In addition, the formation of the long-strained σ -CC bonds between two radical centres has been monitored by calculating the potential energy curve of the dimerization (Figure 2b), which shows a well-defined minimum at 1.65 Å and changes curvature around 2.0-2.1 Å. This calculated C–C bond length is significantly elongated as compared to canonical C(sp³)-C(sp³) bonds (1.54 Å). The σ -bonding between the chains causes the hybridization of the dicyano groups to change from the planar sp² π -character to sp³.¹⁹ The negative estimated energy for the formation of this long C–C single bonds (*i.e.*, -67.8 kcal mol⁻¹) is in agreement with the spontaneous dimerization observed experimentally.

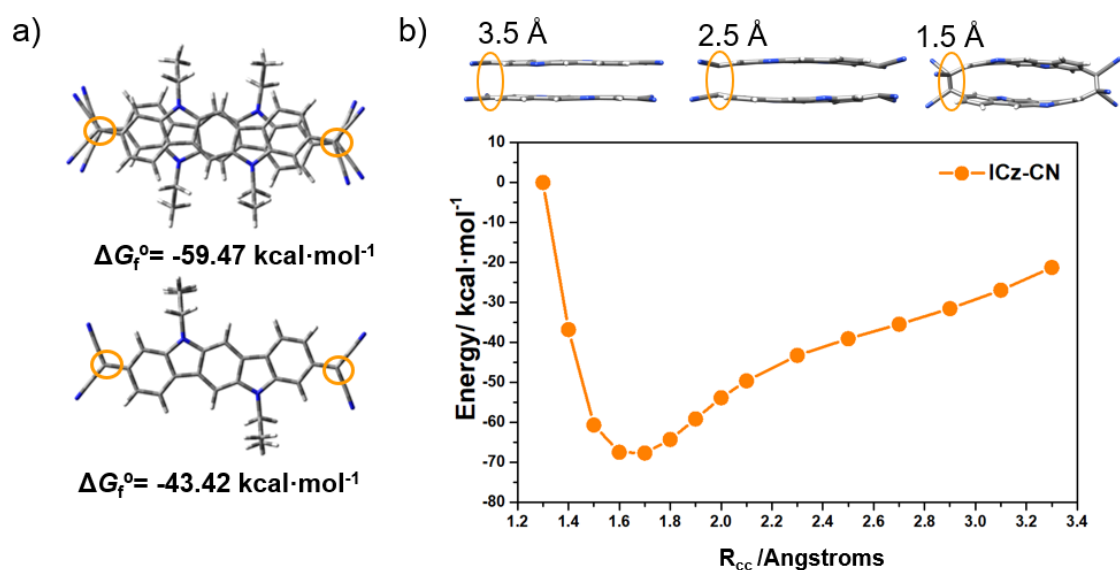


Figure 2. (a) DFT-calculated global-minimum structure for (ICz-CN)₂ in two different configurations: antiparallel (up) and parallel (down) for the spatial arrangement of the two isolated monomers. Free energy of formation values (at 298 K), calculated at the UM06-2X-D3/6-31G** level, are also shown. (b) Relaxed potential energy curve, computed at the UM06-2X/6-31G** level, for (ICz-CN)₂. Here R_{cc} is the length of the C–C σ -bonds formed between two **ICz-CN** monomers.

3. Diradical Character Investigation

To gain a deeper insight into the electronic structure and the diradical character of the **ICz-CN**, geometry optimizations at the density functional theory (DFT) level were carried out. Herein, the HOMO and LUMO distributions from the closed-shell state exhibit a delocalization over the whole π -conjugated backbone. Comparing the **ICz-CN** compound with its short-chain analogue **Cz-CN**,^{3b} the elongation of the conjugated core causes the destabilization of the HOMO while the LUMO is slightly affected (as shown in Figure 3a). Consequently, the energy gap decreases²⁰ which, nevertheless, may head to relatively smaller ΔE_{ST} values (5.21 eV in **Cz-CN** vs 1.66 eV in **ICz-CN**, see Table S1); note that **ICz-CN** is an open-shell diradical in the ground electronic state as in the case of **Cz-CN**. The singly occupied molecular orbital (SOMO) profiles of the α and β spatial distribution

present a typical disjointed feature and the resulting spin density distribution, which has a central symmetry, is highly distributed through the whole **ICz-CN** core with a strong contribution from the dicyanomethylene groups (see Figure 3b and 3c). The high spin density over the bridgehead carbon atoms suggests that the connection between the unpaired electrons of the dicyanomethylene groups at the different **ICz-CN** halves should be favoured as a consequence of the increased diradical character.^{3c} The optimized structure of **ICz-CN** reveals that the closed-shell form presents a quinoidal character whereas the open-shell singlet state displays a certain degree of aromatization, mainly localized on the central phenylene ring and the adjacent pyrrole groups (see the calculated bond lengths shown in Figure 4a) which might act as the driving force for the stabilization of the diradical species.

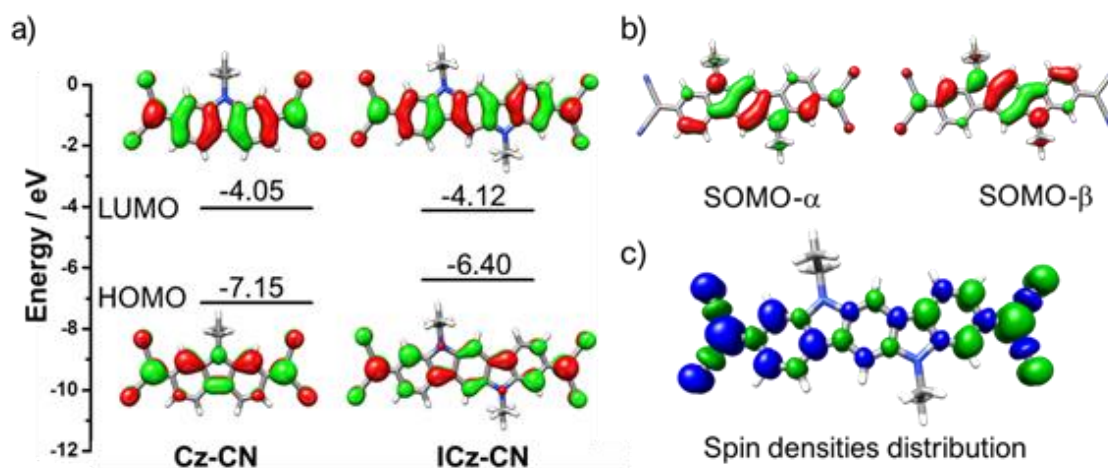


Figure 3. (a) DFT-calculated molecular orbital diagram for **ICz-CN** and **Cz-CN**, the short-chain analogue, at the M06-2X/6-31G** level of theory. (b) Calculated SOMO of α and β electrons and (c) spin density distribution in the diradical singlet ground state of **ICz-CN** at the UM06-2X/6-31G** level of theory with an isosurface value of 0.03 a.u. The blue and green surfaces represent α and β spin densities, respectively.

We now shall address the diradical character of the **ICz-CN** compound which gives a quantitative evaluation of its open-shell singlet nature. This parameter was obtained by using the following methods: (i) through the occupation number of the lowest unoccupied natural orbital (LUNO) ($0 < y_0 < 1$, where $y_0 = 0$ represents a closed-shell state and $y_0 = 1$ represents a pure diradical state), (ii) from the spin-projected formalism, and (iii) using the fractional orbital density (FOD) analysis where the number of strongly correlated electrons in the system is measured. For **ICz-CN**, we obtained values of $N_{\text{FOD}} = 1.95$ together with $y_0 = 0.79$ and $y_0 = 0.61$, without and with spin-projected correction, respectively. However, note that smaller N_{FOD} and y_0 values (*i.e.*, 1.31 and 0.49, respectively) are predicted for the carbazole analogue, **Cz-CN** system.^{3b} A linear relationship between the experimental diradical character and the N_{FOD} values was described by Bauer and co-workers for some polyaromatic hydrocarbons (PAHs),²¹ as shown in Figure S6. These data reveal that N_{FOD} values larger than 1.5 confirm a greatly pronounced diradical character. In addition, the FOD-density plot, shown in Figure 4b, displays a strong contribution from the carbon atoms of the dicyanomethylene groups which support the radicals in the open-shell resonance structure. In summary, this strong diradical character together with the small above-mentioned OS singlet-triplet gap indicates a very weak coupling between the two radical sites in **ICz-CN**.

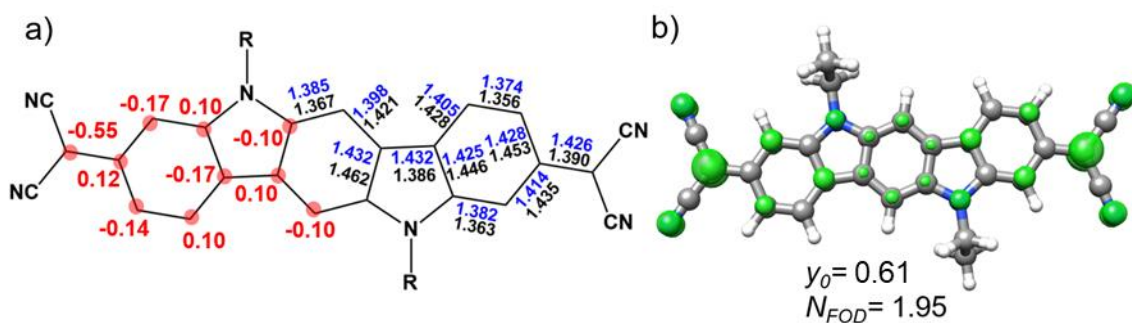


Figure 4. (a) Calculated bond lengths (Å) for the closed-shell (black data) and open-shell singlet (blue data) diradical forms of the ground electronic state of **ICz-CN**. The numbers given in red denote the spin densities at the specific carbon atoms. (b) Isocontour plot of the FOD density ($\sigma = 0.005 \text{ e-bohr}^3$) and predicted NFOD values for **ICz-CN**. The diradical character y_0 values calculated at the (U)M06-2X-631G** level is also shown.

When comparing ^1H NMR spectra **ICz-Br** with that of $(\text{ICz-CN})_2$ (Figure S3) the proton signals of the σ -aggregate are slightly broader, which is ascribed to the presence of a small amount of the open-shell diradical form of monomer **ICz-CN**. In line with further dissociation of $(\text{ICz-CN})_2$ to monomer **ICz-CN** at high temperature, in tetrachloroethene- d_4 (as discussed below), the proton signals in at low field broaden gradually and disappear at 130 °C. Notably, the original spectrum is fully recovered after cooling down the solution back to room temperature.

4. Cyclophane/monomer interconversion in solution

A. Optical properties

Aiming to analyze the influence of different solvents to isolate the monomers, the optical properties of the target samples were monitored by UV-Vis absorption spectroscopy. First, we checked the response as a function of time when the dimer is dissolved in chloroform. As seen in Figure 5a, the freshly prepared chloroform solution displays: i) strong bands in the UV region and medium-weak bands below 500 nm which corresponds to the cyclophane aggregates, and ii) a small and broad absorption at around 700 nm which is ascribed to the isolated monomer. The spectral profile is slightly affected as a function of time.

Second, we investigated the cyclophane/monomer interconversion upon heating. To this end, we dissolved the indolocarbazole compound in toluene (Figure 5b) and heated the solution from 300 K to 380 K. This induces an increase in the intensity of the **ICz-CN** monomer structured band at 700 nm. Nevertheless, the strongest intensity gain of the monomer low-energy visible band was achieved in *o*-dichlorobenzene (*o*-DCB) and tetrachloroethane upon heating (see Figure 5c and Figure S7b, respectively). In fact, almost complete disappearance of the intense UV absorption corresponding to the cyclophane aggregate $(\text{ICz-CN})_2$ is achieved while the **ICz-CN** monomer absorption dominates in the spectrum. Visually, the rupture of the long C–C σ -bonds in the aggregate upon heating is accompanied by a gradual change of the solution colour from light yellow to blue-green, which is fully reversed by cooling down the solution back to 300 K (Figure 5d and Figure S8). A similar behavior was recorded in tetrachloroethane (Figure S8b). On the other hand, the diradical monomer formation was hampered in chlorobenzene and 2-methyltetrahydrofuran (Figure S7). Based in these observations,

o-DCB was selected for the temperature-controlled cyclic voltammetric study of **(ICz-CN)₂** and **ICz-CN** presented in the following section.

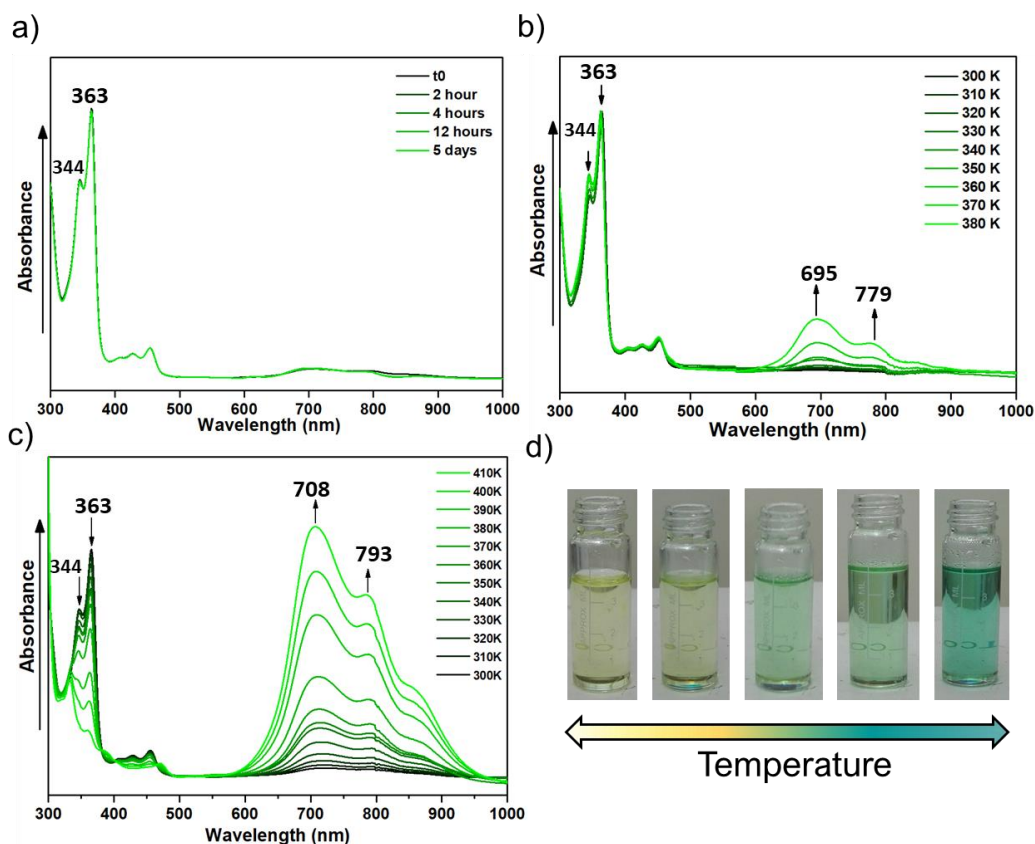


Figure 5. (a) UV-Vis absorption of the freshly prepared solution of **(ICz-CN)₂** in chloroform at room temperature as a function of time. (b) UV-Vis-NIR spectral changes accompanying the thermal conversion of **(ICz-CN)₂** to monomer **ICz-CN** in toluene upon heating. (c) UV-Vis-NIR spectral changes accompanying the nearly complete transformation of **(ICz-CN)₂** to **ICz-CN** in *o*-dichlorobenzene (*o*-DCB) as a function of temperature. (d) Gradual and reversible colour change from light yellow to blue-green upon heating, which reflects the spectral changes in (c).

TD-DFT calculations eminently support the experimental UV-vis spectral evolution when going from the co-facial σ -dimer **(ICz-CN)₂** to the isolated monomer **ICz-CN** (Figures S9 and S10). While a moderate electronic transition at 302 nm together with two less intense transitions at 352 and 371 nm are predicted for **(ICz-CN)₂** corresponding to $S_0 \rightarrow S_5$, $S_0 \rightarrow S_2$ and $S_0 \rightarrow S_1$ transitions, respectively, that involves orbitals with π -character delocalized through the two indolocarbazole moieties, an intense electronic transition at 703 nm is predicted for the isolated monomer **ICz-CN**, which is ascribed to the $S_0 \rightarrow S_2$ transition with a strong $\pi-\pi^*$ character (HOMO \rightarrow LUMO). These results are in good agreement with the HOMO-LUMO gap strongly decreasing when going from **(ICz-CN)₂** to **ICz-CN** (Figure S11). Interestingly, the UV-vis spectrum predicted for the precursor **ICz-Br** resembles that of the aggregate **(ICz-CN)₂**. This is in consonance with the similar energy levels and topologies of the frontier molecular orbitals of **ICz-Br** and **(ICz-CN)₂** (Figures S10 and S11), which suggest an aromatic-to-quinoidal transformation of the π -conjugated indolocarbazole unit upon the HOMO-LUMO optical excitation, whereas an opposite quinoidal-to-aromatic transformation takes place in **ICz-CN** (Figure 3).

B. Redox properties

Redox properties of the **ICz-CN** species, existing at ambient conditions in the dominant cyclophane-type dimeric form, **(ICz-CN)₂**, were investigated with cyclic voltammetry in dichloromethane (DCM) at 298 K (Figure 6), and in 1,2-dichlorobenzene (o-DCB) at 298 and 393 K (Figure S12). Precursor **ICz-Br** was also measured as the reference system. The redox potentials are summarised in Table 2.

For reference **ICz-Br** in DCM, two reversible one-electron oxidations, O1 and O2, are observed at $E_{1/2} = +0.45$ and $+1.09$ V against Fc/Fc⁺. Figure S10 reveals that the π HOMO of **ICz-Br** is fully delocalized over the ICz backbone. The inherent stability of **[ICz-Br]⁺** and the corresponding dication has been confirmed by spectroelectrochemical experiments described in the following section. The reversible oxidation of **(ICz-CN)₂** is shifted positively by 180 mV, which can be attributed to the electron-withdrawing effect of the terminal dicyanomethylene groups, despite their negligible contribution to the HOMO character (Figure S10). This shift is in a good agreement with the slight stabilization of the HOMO when going from **ICz-Br** to **(ICz-CN)₂** (Figure S11). The second oxidation of **(ICz-CN)₂** was not observed within the anodic potential window of the electrolyte. The HOMO of the dimer is delocalized over both σ -bound and π -interacting ICz backbones, which debars the assignment of **[(ICz-CN)₂]⁺** as a redox-asymmetric, mixed-valence species. A strong supportive evidence for this statement has been obtained from the analysis of the UV-Vis-NIR absorption of the cationic product supported by TD-DFT calculations.

The anodic behaviour of **(ICz-CN)₂** and reference **ICz-Br** remains unchanged in o-DCB at 298 K. At 393 K, yellow **(ICz-CN)₂** is fully converted to green diradical **ICz-CN** (Figure S13). The oxidation wave of the monomer becomes irreversible whilst the stability of singly oxidized **[ICz-Br]⁺** is preserved at the elevated temperature. No spectroelectrochemical evidence for the likely decomposition of **[ICz-CN]⁺** could be obtained.

The stabilizing effect of the dicyanomethylene terminal groups on the LUMO of **(ICz-CN)₂** is responsible for the appearance of the cathodic wave of the dimer at $E_{p,c} = -0.81$ V (Figure 6), while no reduction of reference **ICz-Br** was encountered in this cathodic region. The low-lying reduction potential of **(ICz-CN)₂** compared to **ICz-Br** is corroborated by the stabilized LUMO and LUMO+1 levels of the dimer resulting from DFT-calculations (Figure S11). However, the cathodic CV response of the dimer is not straightforward. The reduction wave may appear less resolved at the initial cathodic scan and eventually shifted more negatively by ca. 200 mV. At the same time, it is considerably separated from the anodic counterwave at $E_{p,a} = -0.36$ V preceded by a sharper adsorption wave at -0.54 V. This complicated behaviour is tentatively ascribed to solubility issues and a strong (possibly dissociative) interaction with the Pt cathodic surface. It must not be forgotten that **(ICz-CN)₂** and **ICz-CN** co-exist in an equilibrium at ambient conditions (Figure S4a). The solubility of **(ICz-CN)₂** is lower in o-DCB at 298 K and, indeed, no well-defined cathodic wave is seen in this electrolyte. On the other hand, diradical **ICz-CN** formed in o-DCB at 393 K (Figure S13) undergoes two reversible cathodic steps at $E_{1/2} = -0.46$ and -0.67 V. These values correlate with the low energy of the LUMO of **ICz-CN** determined by DFT calculations (Figure S11). Similar close low-lying cathodic waves were ascertained also in the thin-layer cyclic voltammogram of **(ICz-CN)₂** recorded at 298 K during the follow-up UV-Vis-NIR spectroelectrochemical study (see below). This observation indicates a broken equilibrium between the neutral dimer and monomer induced by the reduction of the minor monomer component.

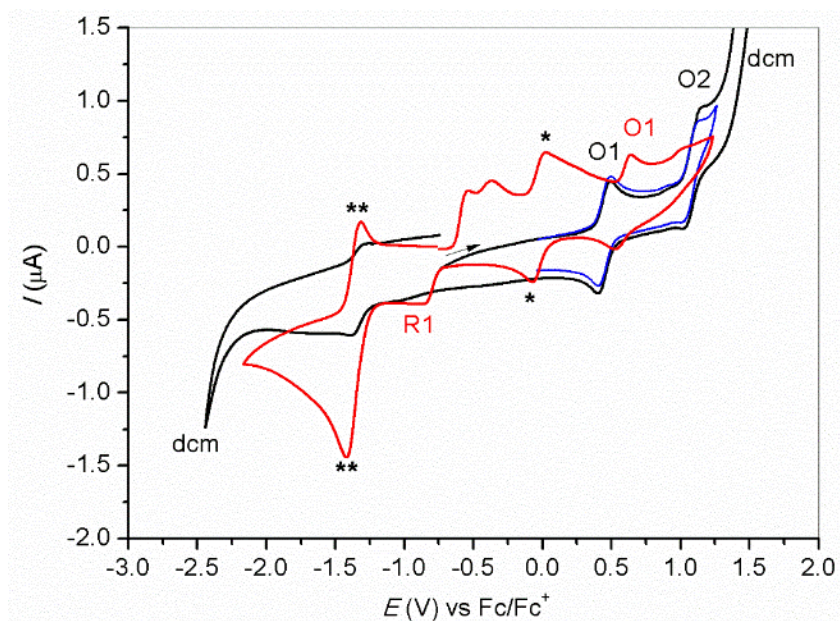


Figure 6. Cyclic voltammograms of 10^{-3} M **ICz-Br** (blue and black curves) and **(ICz-CN)₂** (red curve) in dichloromethane/ Bu_4NPF_6 at a Pt microdisc electrode and $v = 100 \text{ mV s}^{-1}$ and $T = 298 \text{ K}$. The standard ferrocene/ferrocenium (at 0 V, *) and cobaltocene/cobaltocenium (at -1.33 V, **) redox couples were used as the internal references.

Table 2. Redox properties of **ICz-Br**, isolated monomer **ICz-CN** and cyclophane-type dimer **(ICz-CN)₂** determined by cyclic voltammetry at a Pt microdisc.

Compound	$E_{1/2}(1) / \text{V}$	$E_{1/2}(2) / \text{V}$	$E_{1/2}(3) / \text{V}$
ICz-Br	0.45 (O1) ^a	1.09 (O2) ^a	-
	0.44 ^b	1.08	-
	0.45 ^c	^d	-
(ICz-CN)₂	0.63 ^a	^d	-0.86 ^{a,e}
	0.60 ^b	^d	-
ICz-CN	0.70 ^{c,f}	^d	-0.46, -0.67 (R1, R2) ^c

^a Dichloromethane/ Bu_4NPF_6 at $T = 298 \text{ K}$. ^b *o*-Dichlorobenzene/ Bu_4NPF_6 at $T = 298 \text{ K}$. ^c *o*-Dichlorobenzene/ Bu_4NPF_6 at $T = 393 \text{ K}$. ^d Beyond the anodic potential limit of the electrolyte. ^e $E_{p,c}$, value. ^f $E_{p,a}$, value; irreversible oxidation.

C. UV-Vis-NIR Spectro-electrochemistry

To further probe the nature of the redox steps at ambient temperature pertaining to the indolocarbazole species, cyclophane **(ICz-CN)₂** and reference **ICz-Br**, UV-Vis-NIR

spectroelectrochemistry in DCM was implemented.²² Table 3 summarises the positions of electronic absorption maxima for both species in the varying oxidation states.

Table 3. Electronic absorption of **ICz-Br** and **(ICz-CN)₂**, and their stable redox forms in DCM at 298 K.

Compound	ICz-Br	(ICz-CN) ₂
Neutral Parent	290, 333, 350, 402, 422	296, 346, 364, 427, 456
Radical Cation	324, 342, 404, 871	328, 348, 411, 852
Dication	314, 609	-
Radical Anion ^a	-	292, 451, 570
Dianion ^a	-	290, 442, 568

^a Corresponds to stable reduced monomer **ICz-CN**.

The reversible UV-Vis spectral changes accompanying the smooth two-step oxidation of reference **ICz-Br** to the corresponding monocationic and dicationic states (Table 3) are shown in Figures S15 and S16, respectively. The same isosbestic points are maintained during the corresponding reverse cathodic steps and the intermediate cationic and parent absorptions are fully recovered. The experimental electronic absorption of **[ICz-Br]⁺** in the UV-Vis-NIR is plausibly reproduced by TD-DFT calculations (Figure S17, Table S3).

Comparing the reversible one-electron oxidation of the cyclophane dimer **(ICz-CN)₂**, a very similar response is seen in Figure 7. This observation specifically regards the appearance of the new structured band at 328/348/411 nm and the NIR absorption maximum at ca. 852 nm. These absorption features are fairly well reproduced by TD-DFT calculations on **[(ICz-CN)₂]⁺** (Figure S17). The dimer cation does not absorb between 500-600 nm, differently from **[ICz-Br]⁺** that show a weak absorption in that region (Figure S15). In contrast, strong absorption around 500 nm has been predicted for singly oxidized monomer **[ICz-CN]⁺** (Table S3). Thus, the recorded experimental SEC spectra (Figure 7) comply with the dimeric cyclophane structure preserved at ambient temperature also in the oxidized product, in line with the reversible nature of the anodic process. Both **[ICz-Br]⁺** and spin-delocalized **[(ICz-CN)₂]⁺** (cf. the HOMO of the parent compound in Figure S10) apparently feature similar chromophores largely independent of the terminal substituents. This coincidence has a likely origin in the similar aromatic nature of the ICz backbone in both compounds, as the CN groups are no longer π -conjugated with the ICz core upon the formation of the long C-C σ -bonds.

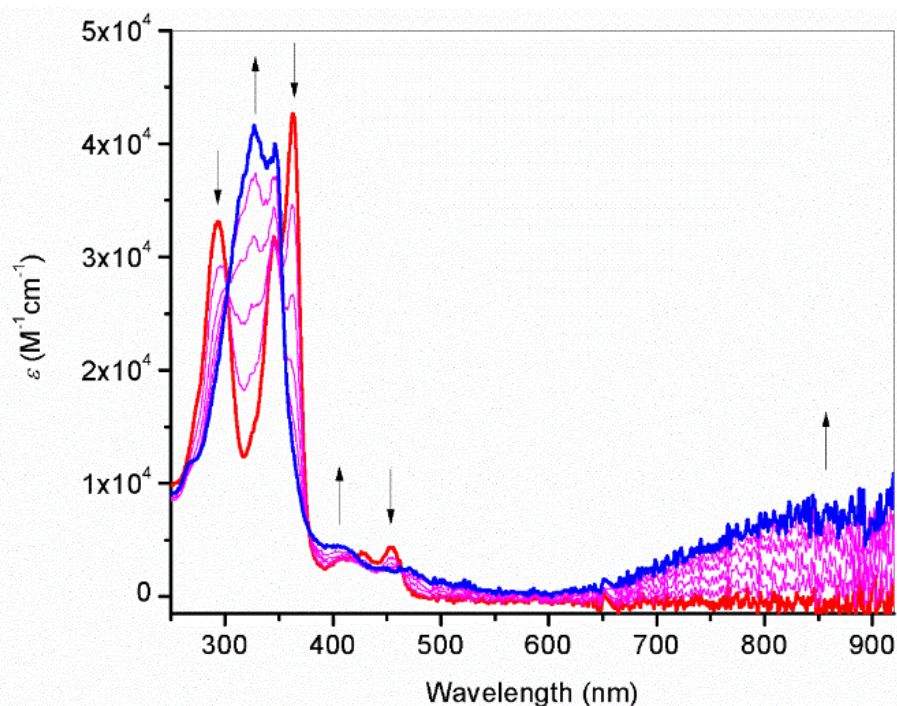


Figure 7. UV-Vis spectral changes recorded during the reversible oxidation $(\text{ICz-CN})_2 - e^- \rightarrow [(\text{ICz-CN})_2]^+$ in $\text{CH}_2\text{Cl}_2/10^{-1} \text{ M Bu}_4\text{NPF}_6$ at 298 K within an OTTLE cell.

In contrast to **ICz-Br**, diradical **ICz-CN** is reducible in two fully reversible one-electron steps at low overpotentials (Table 2). At ambient temperature, **ICz-CN** presents only a minor component in the equilibrium with the cyclophane dimer (Figure S4a) and its conventional CV could only be recorded at sufficiently high temperatures where the cyclophane dimer fully dissociates (Figure S12). However, the thin-layer CV of $(\text{ICz-CN})_2$ recorded in dichloromethane at ambient temperature showed two close-lying, reversible cathodic waves at low electrode potentials resembling the cathodic response of monomer **ICz-CN** whose LUMO is strongly stabilized compared to the dimer (Figure S11). Therefore, the cathodic spectroelectrochemistry of $(\text{ICz-CN})_2$ in fact started with the reduction of the minor diradical component of the mixture, having converted the dimer completely to the singly reduced monomer, $[\text{ICz-CN}]^-$. The second cathodic step then produces stable $[\text{ICz-CN}]^{2-}$. The corresponding UV-Vis spectral changes accompanying both reduction steps are depicted in Figure 8. The presence of isosbestic points excludes any side reaction. A full recovery of the parent dimer absorption was observed after the stepwise reoxidation of $[\text{ICz-CN}]^{2-}$, in line with the reversible nature of the thin-layer CV trace recorded in parallel with the spectral monitoring. The anion $[\text{ICz-CN}]^-$ features a new strong and broad absorption band with a maximum at 451 nm, and a weaker absorption at 570 nm. This visible absorption persists also in the dianion $[\text{ICz-CN}]^{2-}$ but both the intensity and bandwidth are affected. Electronic transitions of $[\text{ICz-CN}]^-$ and $[\text{ICz-CN}]^{2-}$ in the near UV-visible region calculated with TD-DFT (Figure S17) are consistent with the experimental spectra, reproducing the intense electronic absorption around 450 nm measured for $[\text{ICz-CN}]^-$ and its increased intensity when generating $[\text{ICz-CN}]^{2-}$. The weak absorption features of the reduced forms of **ICz-CN** between 500-650 nm were, however, not reproduced. On the other hand, the modelled reduced dimers, $[(\text{ICz-CN})_2]^{n-}$ ($n = 1, 2$), differ strongly in the calculated electronic absorption, showing strong low-energy absorptions at 864 nm (anion) and 708 nm (dianion) not encountered in the experimental spectra. The combined voltammetric and spectral evidence leads to the conclusion that the cyclophane structure dominates in the solution and ambient

conditions only in the neutral state. The cathodic spectroelectrochemistry confirms the existence of the equilibrium between **ICz-CN** and **(ICz-CN)₂** revealed by other methods (Figures S3 and S4), starting with the reduction of the minor monomer component at the characteristic low electrode overpotential. The broken equilibrium caused by the electron transfer converts the cyclophane dimer readily to the monomer anion that undergoes the second reversible reduction. Reversely, the reoxidation of **[ICz-CN]⁻** to the neutral diradical restores the equilibrium with the dominant cyclophane dimer. It would have been even more conclusive to conduct the reversible reduction of isolated diradical **ICz-CN** in *o*-dichlorobenzene at 393 K (Figure S12) but the experimental setup for this experiment was not at disposal.

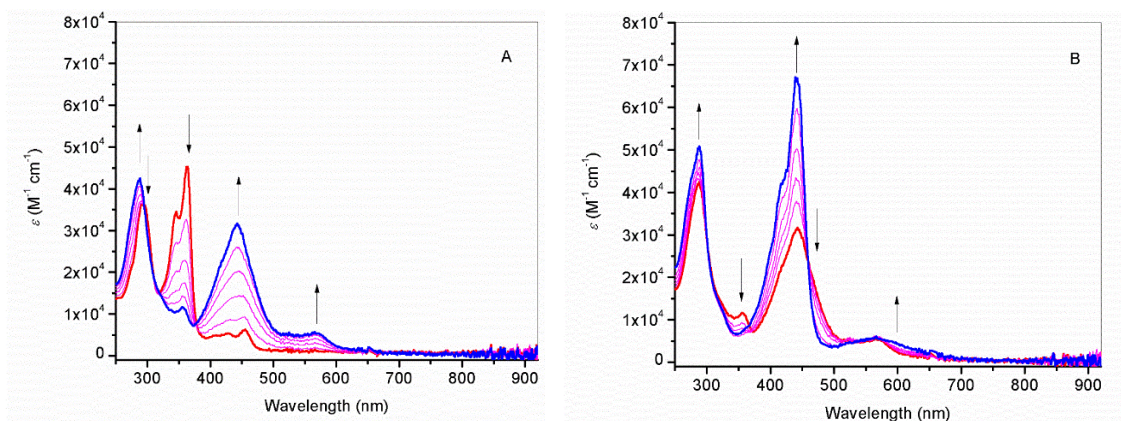


Figure 8. UV-Vis spectral changes recorded during the cathodic steps 1/2 **(ICz-CN)₂ + e⁻ → [ICz-CN]⁻** (A) and **[ICz-CN]⁻ + e⁻ → [ICz-CN]²⁻** (B) in CH₂Cl₂/10⁻¹ M Bu₄NPF₆ at 298 K within an OTTE cell.

5. Cyclophane/monomer interconversion in the solid state: temperature and pressure dependence

The C–C σ -bond dissociation in the solid state of the cyclophane dimer was attempted by application of external stimuli such as elevated temperature or pressure. To this end, we have used IR and Raman spectroscopies to probe structural effects causing any mechanochromic changes^{3b, c, 19, 23} and for the investigation of the diradical character of quinoidal molecules.²⁴

Upon application of mechanical stimuli, *i.e.*, grinding of **(ICz-CN)₂** powder with a mortar to prepare a KBr pellet for IR spectroscopy (estimated maximum pressure/stress *ca.* 0.1 GPa), a slight darkening is observed (Figure 9a). This observation suggests that mild pressures have modest impact on the cyclophane dimer/monomer transformation, as further corroborated by IR spectroscopy. The most intense $\nu(\text{CN})$ band, attributed to the cyclophane light-yellow powder at ambient conditions, appears centred at 2255 cm⁻¹ (similar to non-conjugated nitriles). This band remains prominent in the IR spectrum of the corresponding KBr pellet recorded at both room temperature and 523 K and then cooled down back to room temperature, thus suggesting that the dimer cyclophane structure is always prevalent. However, two additional weak $\nu(\text{CN})$ features appear after grinding at *ca.* 2224 and 2189 cm⁻¹, which is attributed to the formation of isolated monomers **ICz-CN** and open linear staircase dimers, **(ICz-CN)₂-op**, with two unpaired electrons at the terminals, respectively. This assignment is strongly supported by DFT

calculations of the corresponding structures (Figure 9b and Figure S18). In contrast, the σ -aggregates formed by the analogous carbazole-based **Cz-CN** systems dissociate much easier in the solid state^{3b, c}; this difference is ascribed to the longer conjugated ICz backbones enabling stronger π - π interactions between the co-facially overlapped cores in the pancake (**ICz-CN**)₂ aggregates.

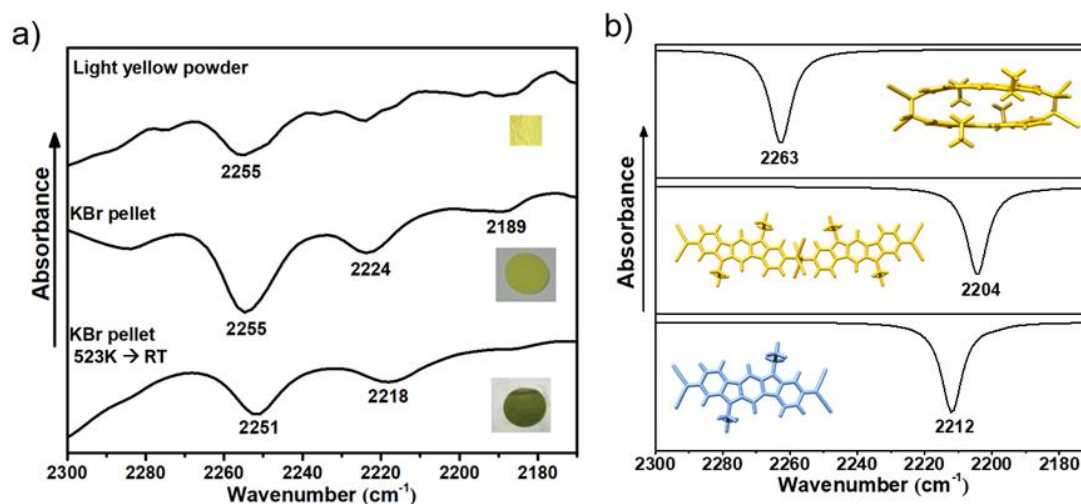


Figure 9. (a) IR spectrum of (**ICz-CN**)₂ as a light-yellow powder at room temperature (top), a yellow KBr pellet containing a mixture of dimer, open linear oligomer and isolated diradical **ICz-CN** (middle), and the KBr pellet after heating at 523 K (bottom). (b) Theoretical IR spectra of (**ICz-CN**)₂ (top), open linear (**ICz-CN**)₂-op (middle) and **ICz-CN** monomer (bottom).

Figure 10a displays the FT-Raman spectrum of the light-yellow powder corresponding to the (**ICz-CN**)₂ dimer aggregate, and the resonance Raman spectrum of isolated diradical **ICz-CN** in *o*-DCB at 363 K. When comparing the two spectra, the most pronounced changes are found in the fingerprint region between 1700 and 1100 cm⁻¹. (i) The most intense band of the dimeric structure appears at 1640 cm⁻¹, assigned to a ν (CC) mode of the ICz rings (notice that is quite similar to that assigned to the aromatic precursor **ICz-Br** at 1634 cm⁻¹) (ii) Notably, this ν (CC) mode appears at 1580 cm⁻¹ in the isolated monomer, thus suggesting a change in the molecular structure from an aromatic to a more quinoidal character. (iii) The appearance of the band at 1191 cm⁻¹ in the resonance Raman spectrum of hot solution corroborates the presence of the isolated **ICz-CN** monomer structure, as this mode is ascribed to the CH bending of the central phenylene ring being hindered in the dimeric unit. This experimental spectral evolution is in a very good agreement with the theoretical Raman spectra (Figure 10b); for instance, in the calculated spectra of the **ICz-CN** isolated monomer the two key bands indicating the diradical monomer formation are predicted at 1574 and 1195 cm⁻¹.

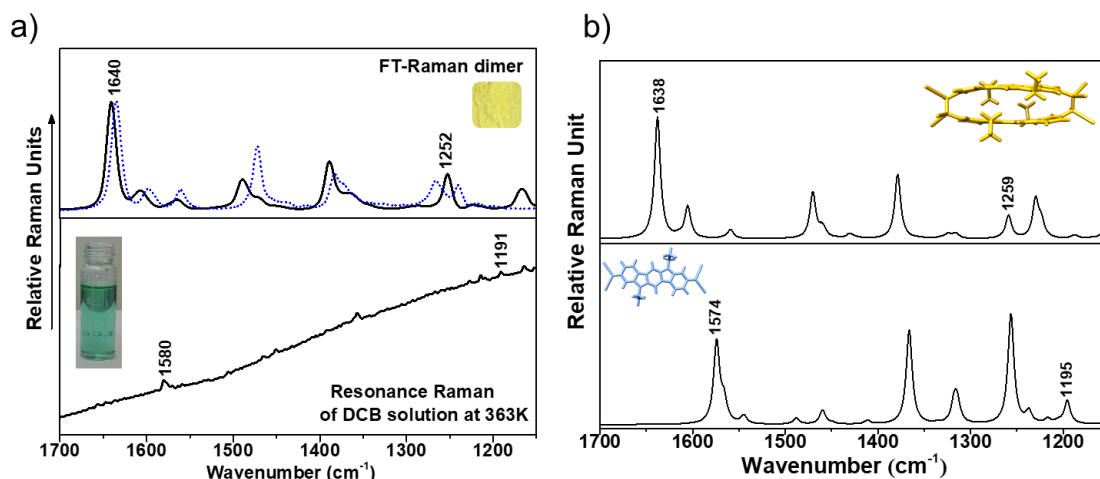


Figure 10. (a) FT-Raman spectra of the solid yellow powder of $(\text{ICz-CN})_2$ (black line) and brominated precursor ICz-Br plotted as blue dots (top) and the resonance Raman spectrum ($\lambda_{\text{exc}} = 785 \text{ nm}$) of isolated diradical ICz-CN in *o*-DCB at 363 K (bottom). (b) Theoretical Raman spectra calculated (M06-2X/6-31G**) for $(\text{ICz-CN})_2$ and ICz-CN .

The transformation of the dimeric cyclophane structure into the isolated monomers in the solid state could also be monitored when applying pressures raising well above 0.1 GPa in a more controlled way.²⁵ To this end, $(\text{ICz-CN})_2$ was compressed by means of a sapphire anvil cell. Raman spectroscopy is an excellent diagnostic tool to evaluate electronic and structural changes in π -conjugated systems, as π -electron density is highly polarizable and consequently, changes in the Raman shift, width and cross section will be highly sensitive to changes in the π -electron density.²⁶ As depicted in Figure 11, at compressions reaching ca. 2.2 GPa, the Raman spectrum reveals several differences from that at the ambient pressure, suggesting that the dimer C–C bonds are broken and a monomer configuration is favoured. This assignment is supported by the appearance of new Raman bands at 1585 cm^{-1} and 1140 cm^{-1} . As previously mentioned, the band ca. 1580 cm^{-1} is linked to the $\nu(\text{CC})$ stretching mode of the conjugated core in the monomer, while the band at 1140 cm^{-1} corresponds to the $w(\text{CC})$ (wagging) mode of the central phenylene unit. The latter mode becomes intense in the monomer because it is not hindered by the neighbouring connecting unit, as observed in the dimer. The colour changes from light-yellow to deep-green observed under the application of pressures in the few GPa range, reflecting the transformation of dimer $(\text{ICz-CN})_2$ to isolated monomer ICz-CN (see Figure S19)

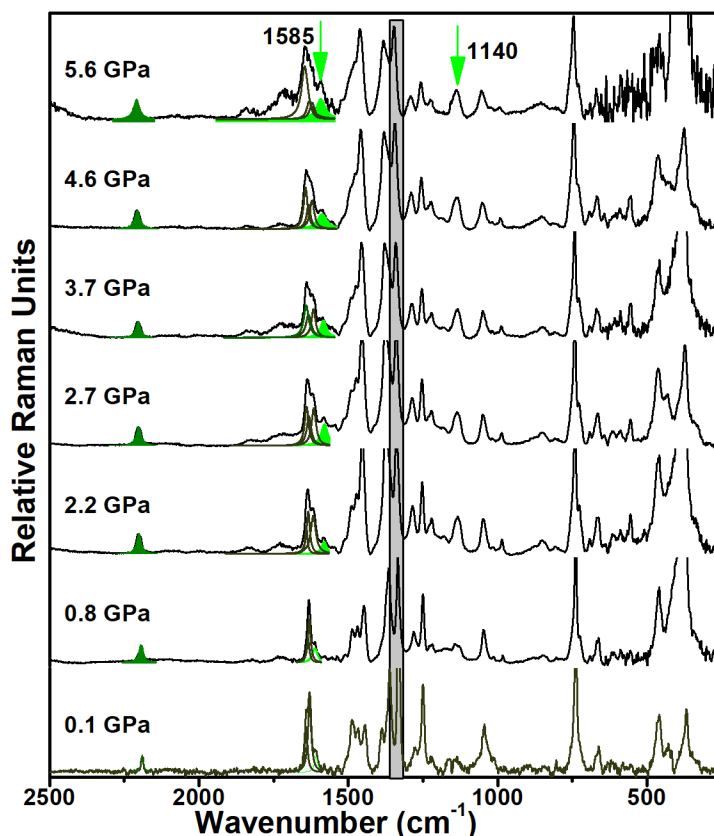


Figure 11. Raman spectra of the solid yellow powder of $(\text{ICz-CN})_2$ at selected pressures measured using the 785 nm as excitation line. Marked peaks correspond to: $\nu(\text{CC})$ stretching mode of the conjugated bonds. The Raman shift of this diamond with compression is used as pressure marker.

Conclusions

This work demonstrates for the first time the dynamic covalent properties of indolocarbazole-based diradicals. To this end, we have synthesized a novel indolo[3,2-b]carbazole substituted with dicyanomethyl groups, **ICz-CN**, which is isolated as a stable σ -dimer $(\text{ICz-CN})_2$. A dynamic equilibrium between the isolated diradical **ICz-CN** and the dimeric cyclophane $(\text{ICz-CN})_2$ is observed in solution at ambient conditions (with a minor diradical component), as proven by HPLC, NMR and cathodic spectroelectrochemistry. Comparing the **ICz-CN** compound with its short-chain carbazole-based analogue, **Cz-CN**, the elongation of the conjugated core results in an increase of the diradical character together with the small open-shell singlet-triplet gap. The weak cyclophane C–C bonds are susceptible to thermal and mechanochemical cleavage both in the solid state and solution, as demonstrated by combining an exhaustive experimental and theoretical approach. Interestingly, the dynamic cyclophane/monomer interconversion is accompanied by a strong colour change from light yellow to blue-green. In summary, this work has shed light on the challenging dynamic covalent chemistry properties of π -conjugated diradicals and helped to identify new potential design strategies for stimuli-responsive materials.

Supporting Information

The following file is available free of charge:

Experimental and Theoretical Methodology; Synthetic details; Related chemical structures; ^1H NMR spectra of **(ICz-CN)₂**, compound **1** and **ICz-Br**; HPLC and GPC data; DFT-computed global minimum structure for **(ICz-CN)₂**; Comparison of experimental diradical character (y_0) and the N_{FOD} data; DFT-calculated relative energies for **ICz-CN** and **Cz-CN** and free energy of formation values for **(ICz-CN)₂** and **ICz-CN**; UV-Vis-NIR absorption of solution of **ICz-CN** in different solvents; TD-DFT calculated vertical transition energies and diagram of the frontier molecular orbital energy levels for **ICz-CN**, **(ICz-CN)₂** and **ICz-Br**; cyclic voltammograms of **(ICz-CN)₂** and **ICz-Br**; Spectroelectrochemical data for **ICz-Br**; TD-DFT calculated vertical transition energies and diagram of the frontier molecular orbital energy levels for **ICz-CN**, **(ICz-CN)₂** and **ICz-Br** in their reduced and oxidized states. and differential-pulsed cyclovoltammograms; DFT-calculated global minimum structure for open linear dimer **(ICz-CN)₂-op**; Colour changes of **(ICz-CN)₂** converting to **ICz-CN** at high pressures; Pressure-dependent Raman spectra of **(ICz-CN)₂**.

ORCID

Irene Badía Domínguez: 0000-0002-2736-8943
Andrés Pérez Guardiola: 0000-0002-8340-1349
Sandra Rodríguez González 0000-0001-6563-7852
Juan Carlos Sancho García: 0000-0003-3867-1697
František Hartl: 0000-0002-7013-5360
M. Carmen Ruiz Delgado: 0000-0001-8180-7153

Notes

The authors declare no competing financial interest.

Acknowledgment

The work at the University of Málaga was funded by the MICINN ((PID2019-110305GB-I00) and Junta de Andalucía (UMA18-FEDERJA-080 and P09FQM-4708) projects. S.R.G. also thanks the Ayuda para la incorporación de doctores of the University of Malaga. The work at the University of Alicante was supported by the MICINN (PID2019-106114GB-I00) and Generalitat Valenciana (AICO/2018/175) projects. The work at SIOC was supported by National Natural Science Foundation of China (Grant Nos. 21875279 and 21790362). The authors thankfully acknowledge the computer resources, technical expertise, and assistance provided by the SCBI (Supercomputing and Bioinformatics) centre of the University of Malaga. The spectro-electrochemical studies (R.N.) were fully funded by Spectroelectrochemistry Reading (a spinout company of the University of Reading). M.P.-A. would like to acknowledge the support of the European Research Council (ERC) Grant “Hecate”, Reference No. 695527, held by Prof. Graeme Ackland. This work has been also supported by MCIU/MINECO through the projects CTQ2013-48252-P, CTQ2015-67755-C02-01-R and PGC2018-094814-B-C21.

References

1. (a) Mutoh, K.; Miyashita, N.; Arai, K.; Abe, J., Turn-On Mode Fluorescence Switch by Using Negative Photochromic Imidazole Dimer. *Journal of the American Chemical Society* **2019**, *141* (14), 5650-5654; (b) Yamaguchi, T.; Hatano, S.; Abe, J., Multistate Photochromism of 1-Phenyl-naphthalene-Bridged Imidazole Dimer That Has Three Colorless Isomers and Two Colored Isomers. *The Journal of Physical Chemistry A* **2014**, *118* (1), 134-143.
2. (a) Oda, K.; Hiroto, S.; Shinokubo, H., NIR mechanochromic behaviours of a tetracyanoethylene-bridged hexa-peri-hexabenzocoronene dimer and trimer through dissociation of C–C bonds. *Journal of Materials Chemistry C* **2017**, *5* (22), 5310-5315; (b) Nagura, K.; Saito, S.; Yusa, H.; Yamawaki, H.; Fujihisa, H.; Sato, H.; Shimoikeda, Y.; Yamaguchi, S., Distinct Responses to Mechanical Grinding and Hydrostatic Pressure in Luminescent Chromism of Tetrathiazolylthiophene. *Journal of the American Chemical Society* **2013**, *135* (28), 10322-10325.
3. (a) Kobashi, T.; Sakamaki, D.; Seki, S., N-Substituted Dicyanomethylphenyl Radicals: Dynamic Covalent Properties and Formation of Stimuli-Responsive Cyclophanes by Self-Assembly. *Angewandte Chemie International Edition* **2016**, *55*(30), 8634-8638; (b) Wang, D.; Capel Ferrón, C.; Li, J.; Gámez-Valenzuela, S.; Ponce Ortiz, R.; López Navarrete, J. T.; Hernández Jolín, V.; Yang, X.; Peña Álvarez, M.; García Baonza, V.; Hartl, F.; Ruiz Delgado, M. C.; Li, H., New Multiresponsive Chromic Soft Materials: Dynamic Interconversion of Short 2,7-Dicyanomethylenecarbazole-Based Biradicaloid and the Corresponding Cyclophane Tetramer. *Chemistry – A European Journal* **2017**, *23* (55), 13776-13783; (c) Badía-Domínguez, I.; Pérez-Guardiola, A.; Sancho-García, J. C.; López Navarrete, J. T.; Hernández Jolín, V.; Li, H.; Sakamaki, D.; Seki, S.; Ruiz Delgado, M. C., Formation of Cyclophane Macrocycles in Carbazole-Based Biradicaloids: Impact of the Dicyanomethylene Substitution Position. *ACS Omega* **2019**, *4* (3), 4761-4769.
4. (a) Zafra, J. L.; Qiu, L.; Yanai, N.; Mori, T.; Nakano, M.; Alvarez, M. P.; Navarrete, J. T. L.; Gómez-García, C. J.; Kertesz, M.; Takimiya, K.; Casado, J., Reversible Dimerization and Polymerization of a Janus Diradical To Produce Labile C–C Bonds and Large Chromic Effects. *Angewandte Chemie International Edition* **2016**, *55* (47), 14563-14568; (b) Yokoi, H.; Hiroto, S.; Shinokubo, H., Reversible σ -Bond Formation in Bowl-Shaped π -Radical Cations: The Effects of Curved and Planar Structures. *Journal of the American Chemical Society* **2018**, *140* (13), 4649-4655; (c) Yuan, L.; Han, Y.; Tao, T.; Phan, H.; Chi, C., Formation of a Macrocycles-in-a-Macrocycle Superstructure with All-gauche Conformation by Reversible Radical Association. *Angewandte Chemie International Edition* **2018**, *57* (29), 9023-9027; (d) Adinarayana, B.; Shimizu, D.; Furukawa, K.; Osuka, A., Stable radical versus reversible σ -bond formation of (porphyrinyl)dicyanomethyl radicals. *Chemical Science* **2019**, *10* (23), 6007-6012; (e) Chen, X.; Wang, X.; Zhou, Z.; Sui, Y.; Sui, Y.; Ma, J.; Wang, X.; Power, P., Reversible σ -Dimerizations of Persistent Organic Radical Cations. *Angewandte Chemie International Edition* **2013**, *52* (2), 589-592; (f) Beaudoin, D.; Levasseur-Grenon, O.; Maris, T.; Wuest, J. D., Building Giant Carbocycles by Reversible C–C Bond Formation. *Angewandte Chemie International Edition* **2016**, *55* (3), 894-898; (g) Moshniaha, L.; Żyła-Karwowska, M.; Chmielewski, P. J.; Lis, T.; Cybińska, J.; Gońka, E.; Oschwald, J.; Drewello, T.; Rivero, S. M.; Casado, J.; Stępień, M., Aromatic Nanosandwich Obtained by σ -Dimerization of a Nanographenoid π -Radical. *Journal of the American Chemical Society* **2020**, *142* (7), 3626-3635; (h) Zhang, R.; Peterson, J. P.; Fischer, L. J.; Ellern, A.; Winter, A. H., Effect of Structure on the Spin–Spin Interactions of Tethered Dicyanomethyl Diradicals. *Journal of the American Chemical Society* **2018**, *140* (43), 14308-14313.

5. (a) Rowan, S. J.; Cantrill, S. J.; Cousins, G. R. L.; Sanders, J. K. M.; Stoddart, J. F., Dynamic Covalent Chemistry. *Angewandte Chemie International Edition* **2002**, *41* (6), 898-952; (b) Lehn, J.-M., From supramolecular chemistry towards constitutional dynamic chemistry and adaptive chemistry. *Chemical Society Reviews* **2007**, *36* (2), 151-160; (c) Sakamaki, D.; Ghosh, S.; Seki, S., Dynamic covalent bonds: approaches from stable radical species. *Materials Chemistry Frontiers* **2019**, *3* (11), 2270-2282.
6. Alcón, I.; Viñes, F.; Moreira, I. d. P. R.; Bromley, S. T., Existence of multi-radical and closed-shell semiconducting states in post-graphene organic Dirac materials. *Nature Communications* **2017**, *8* (1), 1957.
7. (a) Geraskina, M. R.; Buck, A. T.; Winter, A. H., An Organic Spin Crossover Material in Water from a Covalently Linked Radical Dyad. *The Journal of Organic Chemistry* **2014**, *79* (16), 7723-7727; (b) Juetten, M. J.; Buck, A. T.; Winter, A. H., A radical spin on viologen polymers: organic spin crossover materials in water. *Chemical Communications* **2015**, *51* (25), 5516-5519.
8. Jin, Y.; Yu, C.; Denman, R. J.; Zhang, W., Recent advances in dynamic covalent chemistry. *Chemical Society Reviews* **2013**, *42* (16), 6634-6654.
9. (a) Kobashi, T.; Sakamaki, D.; Seki, S., N-Substituted Dicyanomethylphenyl Radicals: Dynamic Covalent Properties and Formation of Stimuli-Responsive Cyclophanes by Self-Assembly. *Angewandte Chemie* **2016**, *128* (30), 8776-8780; (b) Adinarayana, B.; Kato, K.; Shimizu, D.; Tanaka, T.; Furukawa, K.; Osuka, A., Cyclophane-Type Chlorin Dimers from Dynamic Covalent Chemistry of 2,18-Porphyrinyl Dicyanomethyl Diradicals. *Angewandte Chemie* **2020**, *132* (11), 4350-4353; (c) Okino, K.; Sakamaki, D.; Seki, S., Dicyanomethyl Radical-Based Near-Infrared Thermo-chromic Dyes with High Transparency in the Visible Region. *ACS Materials Letters* **2019**, *1* (1), 25-29; (d) Okino, K.; Hira, S.; Inoue, Y.; Sakamaki, D.; Seki, S., The Divergent Dimerization Behavior of N-Substituted Dicyanomethyl Radicals: Dynamically Stabilized versus Stable Radicals. *Angewandte Chemie International Edition* **2017**, *56* (52), 16597-16601; (e) Peterson, J. P.; Ellern, A.; Winter, A. H., Spin Delocalization, Polarization, and London Dispersion Forces Govern the Formation of Diradical Pimers. *Journal of the American Chemical Society* **2020**, *142* (11), 5304-5313; (f) Peterson, J. P.; Winter, A. H., Solvent-Responsive Radical Dimers. *Organic Letters* **2020**, *22* (15), 6072-6076.
10. (a) Zhao, H.; Jiang, L.; Dong, H.; Li, H.; Hu, W.; Ong, B. S., Influence of Intermolecular N \cdots H \cdots π Interactions on Molecular Packing and Field-Effect Performance of Organic Semiconductors. *ChemPhysChem* **2009**, *10* (13), 2345-2348; (b) Ting, H.-C.; Chen, Y.-M.; You, H.-W.; Hung, W.-Y.; Lin, S.-H.; Chaskar, A.; Chou, S.-H.; Chi, Y.; Liu, R.-H.; Wong, K.-T., Indolo[3,2-b]carbazole/benzimidazole hybrid bipolar host materials for highly efficient red, yellow, and green phosphorescent organic light emitting diodes. *Journal of Materials Chemistry* **2012**, *22* (17), 8399-8407; (c) Jia, W.-b.; Wang, H.-w.; Yang, L.-m.; Lu, H.-b.; Kong, L.; Tian, Y.-p.; Tao, X.-t.; Yang, J.-x., Synthesis of two novel indolo[3,2-b]carbazole derivatives with aggregation-enhanced emission property. *Journal of Materials Chemistry C* **2013**, *1* (42), 7092-7101; (d) Boudreault, P.-L. T.; Virkar, A. A.; Bao, Z.; Leclerc, M., Synthesis and characterization of soluble indolo[3,2-b]carbazole derivatives for organic field-effect transistors. *Organic Electronics* **2010**, *11* (10), 1649-1659; (e) Chen, S.; Wei, J.; Wang, K.; Wang, C.; Chen, D.; Liu, Y.; Wang, Y., Constructing high-performance blue, yellow and red electroluminescent devices based on a class of multifunctional organic materials. *Journal of Materials Chemistry C* **2013**, *1* (40), 6594-6602; (f) Reig, M.; Puigdollers, J.; Velasco, D., Molecular order of air-stable p-type organic thin-film transistors by tuning the extension of the π -conjugated core: the cases of indolo[3,2-b]carbazole and triindole semiconductors. *Journal of Materials Chemistry C* **2015**, *3* (3), 506-513; (g) Khetubol, A.; Van Snick, S.; Clark, M. L.; Fron, E.; Coutiño-González, E.; Cloet, A.; Kennes, K.; Firdaus, Y.; Vlasselaer, M.; Leen, V.; Dehaen, W.; Van der Auweraer, M., Improved Spectral Coverage and Fluorescence Quenching in Donor-acceptor Systems Involving Indolo[3-2-b]carbazole and Boron-dipyrromethene or Diketopyrrolopyrrole. *Photochemistry and Photobiology* **2015**, *91* (3), 637-653.

11. Janosik, T.; Rannug, A.; Rannug, U.; Wahlström, N.; Slätt, J.; Bergman, J., Chemistry and Properties of Indolocarbazoles. *Chemical Reviews* **2018**, *118* (18), 9058-9128.
12. (a) Nakano, M.; Kishi, R.; Ohta, S.; Takahashi, H.; Kubo, T.; Kamada, K.; Ohta, K.; Botek, E.; Champagne, B., Relationship between Third-Order Nonlinear Optical Properties and Magnetic Interactions in Open-Shell Systems: A New Paradigm for Nonlinear Optics. *Physical Review Letters* **2007**, *99* (3), 033001; (b) Van Snick, S.; Dehaen, W., Synthesis of novel 2,8-disubstituted indolo[3,2-b]carbazoles. *Organic & Biomolecular Chemistry* **2012**, *10* (1), 79-82; (c) Irgashev, R. A.; Teslenko, A. Y.; Zhilina, E. F.; Schepochkin, A. V.; El'tsov, O. S.; Rusinov, G. L.; Charushin, V. N., Synthesis, photophysical and electrochemical properties of novel 6,12-di(thiophen-2-yl) substituted indolo[3,2-b]carbazoles. *Tetrahedron* **2014**, *70* (31), 4685-4696; (d) Vlasselaer, M.; Dehaen, W., Synthesis of Linearly Fused Benzodipyrrole Based Organic Materials. *Molecules (Basel, Switzerland)* **2016**, *21* (6), 785; (e) Irgashev, R. A.; Kazin, N. A.; Rusinov, G. L.; Charushin, V. N., A convenient synthesis of new 5,11-dihydroindolo[3,2-b]carbazoles bearing thiophene, 2,2' -bithiophene or 2,2' :5',2'' -terthiophene units at C-2 and C-8 positions. *Tetrahedron Letters* **2017**, *58* (32), 3139-3142.
13. (a) Luo, D.; Lee, S.; Zheng, B.; Sun, Z.; Zeng, W.; Huang, K.-W.; Furukawa, K.; Kim, D.; Webster, R. D.; Wu, J., Indolo[2,3-b]carbazoles with tunable ground states: how Clar's aromatic sextet determines the singlet biradical character. *Chemical Science* **2014**, *5* (12), 4944-4952; (b) Yudina, L. N.; Preobrazhenskaya, M. N.; Korolev, A. M., Transformation of 5H,11H-Indolo[3,2-b]carbazole through 5,11-Didehydroindolo[3,2-b]carbazole. *Chemistry of Heterocyclic Compounds* **2000**, *36* (9), 1112-1113.
14. (a) Streckaite, S.; Karpicz, R.; Gruodis, A.; Dehaen, W.; Van Snick, S.; Kirkus, M.; Grigalevicius, S.; Grazulevicius, J. V.; Gulbinas, V., Fluorescence quenching of indolo[3,2-b]carbazole compounds by conformational motions of attached substituents. *Dyes and Pigments* **2016**, *133*, 120-126; (b) Simokaitiene, J.; Stanislovaityte, E.; Grazulevicius, J. V.; Jankauskas, V.; Gu, R.; Dehaen, W.; Hung, Y.-C.; Hsu, C.-P., Synthesis and Properties of Methoxyphenyl-Substituted Derivatives of Indolo[3,2-b]carbazole. *The Journal of Organic Chemistry* **2012**, *77* (11), 4924-4931; (c) Shi, H.; Yuan, J.; Dong, X.; Cheng, F., Synthesis, photophysical and charge-transporting properties of a novel asymmetric indolo [3,2-b]carbazole derivative containing benzothiazole and diphenylamino moieties. *Spectrochimica Acta Part A: Molecular and Biomolecular Spectroscopy* **2014**, *133*, 501-508; (d) Shi, H.-p.; Dai, J.-x.; Wu, X.-h.; Shi, L.-w.; Yuan, J.-d.; Fang, L.; Miao, Y.-q.; Du, X.-g.; Wang, H.; Dong, C., A novel dimesitylboron-substituted indolo[3,2-b]carbazole derivative: Synthesis, electrochemical, photoluminescent and electroluminescent properties. *Organic Electronics* **2013**, *14* (3), 868-874; (e) Bintinger, J.; Yang, S.; Fruhmann, P.; Holzer, B.; Stöger, B.; Svirikova, A.; Marchetti-Deschmann, M.; Horkel, E.; Hametner, C.; Fröhlich, J.; Kymissis, I.; Mikula, H., Synthesis, characterization and printing application of alkylated indolo[3,2-b]carbazoles. *Synthetic Metals* **2017**, *228*, 9-17.
15. (a) Jiménez, V. A.; Gavín, J. A.; Alderete, J. B., Scaling trend in diffusion coefficients of low generation G0–G3 PAMAM dendrimers in aqueous solution at high and neutral pH. *Structural Chemistry* **2012**, *23* (1), 123-128; (b) van Dongen, M. A.; Orr, B. G.; Banaszak Holl, M. M., Diffusion NMR Study of Generation-Five PAMAM Dendrimer Materials. *The Journal of Physical Chemistry B* **2014**, *118* (25), 7195-7202.
16. Fu, X.; Zhao, D., Cyclo-oligomerization of 6,12-Diethynyl Indeno[1,2-b]fluorenes via Diradical Intermediates. *Organic Letters* **2015**, *17* (22), 5694-5697.
17. Wang, D.; Ivanov, M. V.; Kokkin, D.; Loman, J.; Cai, J.-Z.; Reid, S. A.; Rathore, R., The Role of Torsional Dynamics on Hole and Exciton Stabilization in π -Stacked Assemblies: Design of Rigid Torsionomers of a Cofacial Bifluorene. *Angewandte Chemie* **2018**, *130* (27), 8321-8325.
18. Ferrón, C. C.; Capdevila-Cortada, M.; Balster, R.; Hartl, F.; Niu, W.; He, M.; Novoa, J. J.; López Navarrete, J. T.; Hernández, V.; Ruiz Delgado, M. C., Multistep π Dimerization of Tetrakis(n-decyl)heptathienoacene Radical Cations: A Combined

- Experimental and Theoretical Study. *Chemistry – A European Journal* **2014**, *20* (33), 10351-10359.
19. González-Cano, R. C.; Di Motta, S.; Zhu, X.; López Navarrete, J. T.; Tsuji, H.; Nakamura, E.; Negri, F.; Casado, J., Carbon-Bridged Phenylene-Vinylenes: On the Common Diradicaloid Origin of Their Photonic and Chemical Properties. *The Journal of Physical Chemistry C* **2017**, *121* (41), 23141-23148.
20. González Cano, R. C.; Herrera, H.; Segura, J. L.; López Navarrete, J. T.; Ruiz Delgado, M. C.; Casado, J., Conformational Control of the Electronic Properties of an α - β Terthiophene: Lessons from a Precursor Towards Dendritic Hyperbranched Oligo- and Poly-Thiophenes. *ChemPhysChem* **2012**, *13* (17), 3893-3900.
21. Bauer, C. A.; Hansen, A.; Grimme, S., The Fractional Occupation Number Weighted Density as a Versatile Analysis Tool for Molecules with a Complicated Electronic Structure. *Chemistry – A European Journal* **2017**, *23* (25), 6150-6164.
22. Stanger, A., Nucleus-Independent Chemical Shifts (NICS): Distance Dependence and Revised Criteria for Aromaticity and Antiaromaticity. *The Journal of Organic Chemistry* **2006**, *71* (3), 883-893.
23. Mosca, S.; Milani, A.; Peña-Álvarez, M.; Yamaguchi, S.; Hernández, V.; Ruiz Delgado, M. C.; Castiglioni, C., Mechanochromic Luminescent Tetrathiazolythiophenes: Evaluating the Role of Intermolecular Interactions through Pressure and Temperature-Dependent Raman Spectroscopy. *The Journal of Physical Chemistry C* **2018**, *122* (30), 17537-17543.
24. (a) Yang, K.; Zhang, X.; Harbuzaru, A.; Wang, L.; Wang, Y.; Koh, C.; Guo, H.; Shi, Y.; Chen, J.; Sun, H.; Feng, K.; Ruiz Delgado, M. C.; Woo, H. Y.; Ortiz, R. P.; Guo, X., Stable Organic Diradicals Based on Fused Quinoidal Oligothiophene Imides with High Electrical Conductivity. *Journal of the American Chemical Society* **2020**, *142* (9), 4329-4340; (b) Zeng, Z.; Lee, S.; Zafra, J. L.; Ishida, M.; Zhu, X.; Sun, Z.; Ni, Y.; Webster, R. D.; Li, R.-W.; López Navarrete, J. T.; Chi, C.; Ding, J.; Casado, J.; Kim, D.; Wu, J., Tetracyanoquaterrylene and Tetracyanohexarylenequinodimethanes with Tunable Ground States and Strong Near-Infrared Absorption. *Angewandte Chemie International Edition* **2013**, *52* (33), 8561-8565.
25. Baonza, V. G.; Taravillo, M.; Arencibia, A.; Cáceres, M.; Núñez, J., Diamond as pressure sensor in high-pressure Raman spectroscopy using sapphire and other gem anvil cells. *Journal of Raman Spectroscopy* **2003**, *34* (4), 264-270.
26. (a) Alvarez, M. P.; Burrezo, P. M.; Kertesz, M.; Iwamoto, T.; Yamago, S.; Xia, J.; Jasti, R.; Navarrete, J. T. L.; Taravillo, M.; Baonza, V. G.; Casado, J., Properties of Sizeable [n]Cycloparaphenylenes as Molecular Models of Single-Wall Carbon Nanotubes Elucidated by Raman Spectroscopy: Structural and Electron-Transfer Responses under Mechanical Stress. *Angewandte Chemie International Edition* **2014**, *53* (27), 7033-7037; (b) Peña-Alvarez, M.; Qiu, L.; Taravillo, M.; Baonza, V. G.; Delgado, M. C. R.; Yamago, S.; Jasti, R.; Navarrete, J. T. L.; Casado, J.; Kertesz, M., From linear to cyclic oligoparaphenylenes: electronic and molecular changes traced in the vibrational Raman spectra and reformulation of the bond length alternation pattern. *Physical Chemistry Chemical Physics* **2016**, *18* (17), 11683-11692.